ELECTRON-PROTON SCATTERING AT HIGH Q^2
Recent Results and Future Perspectives of Testing QCD and Electroweak Theory at HERA

H.-C. SCHULTZ-COULON
Universität Dortmund, Experimentelle Physik V,
Otto-Hahn-Str. 4, Dortmund, Germany

The e^+p and e^-p scattering data recorded at HERA during the recent years offer the possibility to study electroweak effects in ep interactions apparent at high momentum transfers, Q^2, and to reveal information on the proton parton densities at large values of the Bjorken scaling variable x. From the neutral current cross section measurements, H1 and ZEUS extract the generalized structure function $x\mathcal{F}_3$, which can be related to the valence quark content of the proton. Individual quark densities are extracted by a global fit to the H1 neutral and charged current e^+p and e^-p data. The new results show the sensitivity of high Q^2 ep data to the structure of the proton and indicate what to expect from a 1 fb^{-1} data sample to be taken by H1 and ZEUS until 2006 at the upgraded HERA collider. Future perspectives concerning the investigation of electroweak effects and their utilization to extract the parton content of the proton are shortly discussed.

1 Introduction

At HERA 27.5 GeV positrons collide head on with 920 GeV protons [a], leading to a center-of-mass energy $\sqrt{s}$ of approximately 318 GeV. The HERA facility, with its two collider experiments H1 and ZEUS, therefore offers the unique possibility to probe the structure of the proton down to very small distances ($< 10^{-18}$ m) via t-channel exchange of highly virtual gauge bosons.

The dominant process for deep-inelastic ep scattering (DIS) is given by the exchange of a photon between the incoming lepton and a quark of the proton. However, at high momentum transfers, Q^2, the contributions from neutral (NC) and charged current (CC) reactions with exchange of a massive vector boson, a Z^0 or a $W^\pm$, become important, allowing the investigation

[a] The proton beam energy has been increased from 820 GeV to 920 GeV after the 1997 data taking period; data recorded before 1998 are taken at a center-of-mass energy of 300 GeV.

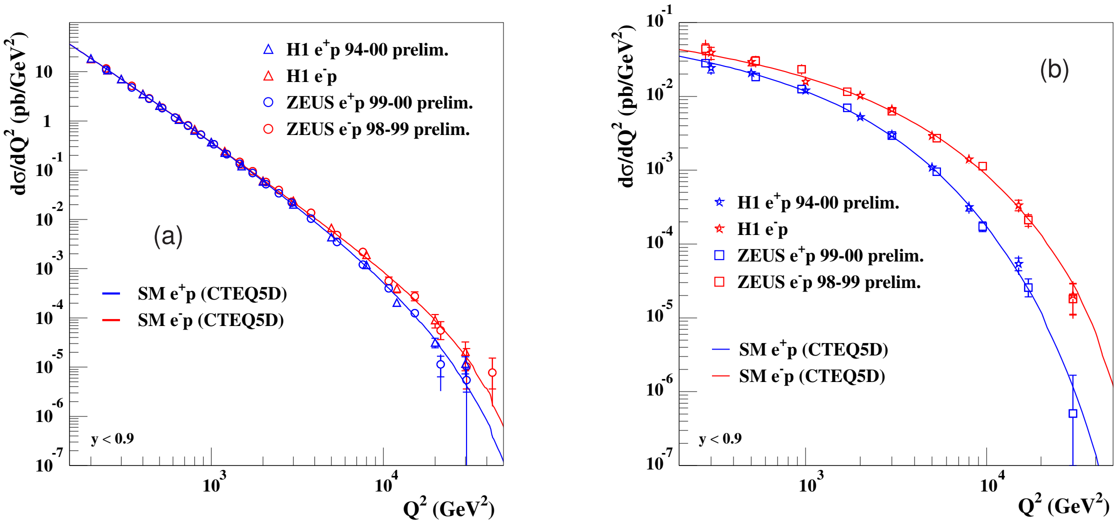

Figure 1: The Q^2 dependence of the NC (a) and CC (b) cross sections, $d\sigma/dQ^2$, for e^+p and e^-p data and the corresponding $\mathcal{SM}$ expectation evaluated using the CTEQ5D [8] parton densities. The statistical uncertainties are indicated by the inner error bars, while the full error bars show the total statistical and systematic uncertainties added in quadrature.

of electroweak effects in lepton-proton reactions. With the statistics collected at HERA until the end of 2000 precise e^+p and e^-p cross section measurements [1−7] have become available, which at high Q^2 clearly reveal the expected dependence on the lepton beam charge predicted by the Standard Model ($\mathcal{SM}$), e.g. an increased NC cross section for e^-p with respect to e^+p scattering due to positive interference between the γ- and Z-exchange. This can be seen from figure 1, which compiles the most recent H1 and ZEUS results for the differential neutral and charged current cross sections, $d\sigma/dQ^2$, reaching values of Q^2 up to 30000 GeV^2.

Exploitation of the observed dependence on the lepton beam charge yield access to information on the valence quark content of the proton at high values of the Bjorken scaling variable x, as will be discussed in the following sections. The data do, however, not yet allow for a precise extraction of electroweak parameters. This will only be possible after the HERA 2 run has been completed, for which a ten-fold increase in statistics is anticipated. Some of the prospects concerning electroweak physics and the determination of parton densities at high Q^2 and high x are considered in section 5.

2 Neutral Current Reactions

The Born cross section [9,10] for the NC DIS reaction $e^\pm p \to e^\pm X$ is given by

$$\frac{d^2\sigma^\pm_{\rm NC}}{dx\,dQ^2} = \frac{2\pi\alpha^2}{xQ^4}\left\{Y_+(y)\,\mathcal{F}_2(x,Q^2) \mp Y_-(y)\,x\mathcal{F}_3(x,Q^2) - y^2\mathcal{F}_L(x,Q^2)\right\} \tag{1}$$

where α is the fine structure constant and the functions $Y_\pm = 1 \pm (1-y)^2$ describe the helicity dependence of the electroweak interactions. The longitudinal structure function $\mathcal{F}_L$ contributes only at high y (i.e. small x and small Q^2 for HERA kinematics) and is neglected in the following discussion [b]. The partonic structure of the proton is then contained in the generalized structure

[b] In general both experiments estimate the $\mathcal{F}_L$ contributions from QCD fits and take them into account when deriving results at very high y or calculating systematic errors. A recent H1 determination [4] of $\mathcal{F}_L$ at high Q^2 shows good agreement between the QCD predictions and the measurement justifying this approach.

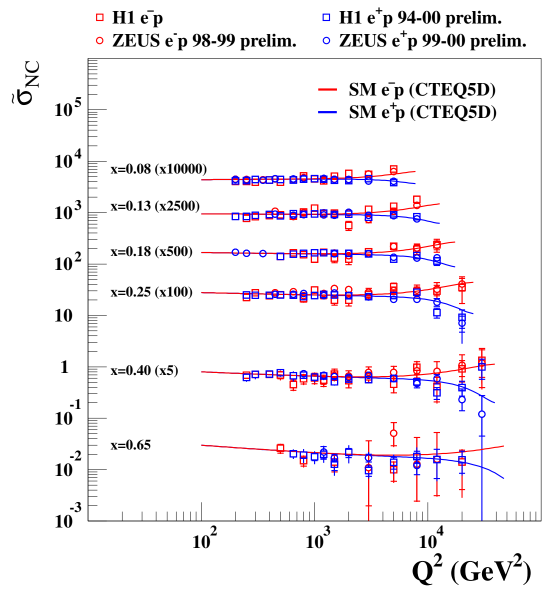

Figure 2: The NC reduced cross section $\tilde{\sigma}_{\rm NC}(x, Q^2)$ at high x compared to the $\mathcal{SM}$ prediction evaluated using the CTEQ5D[8] parton densities. The inner error bars represent the statistical error, and the outer error bars the total error.

functions $\mathcal{F}_2$ and $\mathcal{F}_3$. For unpolarized beams they can be written as

$$\left(\begin{array}{c} \mathcal{F}_2(x,Q^2) \\ x\mathcal{F}_3(x,Q^2) \end{array} \right) = \sum_{q=\text{quarks}} x \left(\begin{array}{cc} C_2^q(Q^2) & [q(x,Q^2) + \bar{q}(x,Q^2)] \\ C_3^q(Q^2) & [q(x,Q^2) - \bar{q}(x,Q^2)] \end{array} \right) . \tag{2}$$

Here, q and $\bar{q}$ are the quark densities depending on x and Q^2 alone, while the coefficient functions C_2^q and C_3^q can be expressed in terms of precisely measured electroweak parameters. In lowest order they are given by

$$C_2^q = e_q^2 - 2e_q v_e v_q \chi_Z + (v_e^2 + a_e^2)(v_q^2 + a_q^2)\chi_Z^2 \tag{3}$$

$$C_3^q = -2e_q a_e a_q \chi_Z + 4 v_e a_e v_q a_q \chi_Z^2 \ , \tag{4}$$

where v_e, v_q and a_e, a_q are the vector and axial couplings of the Z-boson to quarks and electrons, e_q represents the quark charge and $\chi_Z = \kappa_w Q^2/(Q^2 + M_Z^2)$ is the propagator term with $\kappa_w^{-1} = 4\sin^2\theta_W \cos^2\theta_W$. Generally it is convenient to derive the neutral current reduced cross section in which the dominant part of the Q^2 dependence of $d^2\sigma/dxdQ^2$ due to the γ-propagator is removed

$$\tilde{\sigma}_{\rm NC} = \frac{1}{Y_+} \frac{Q^4 x}{2\pi\alpha^2} \frac{d^2\sigma_{\rm NC}}{dxdQ^2} \ . \tag{5}$$

In this form the differences between e^-p and e^+p scattering at high Q^2 are more clearly observed, as can be seen from figure 2. Up to Q^2 values of about 1000 GeV^2 the e^-p data are found to be in agreement with the e^+p measurements as is expected for a solely electromagnetic interaction. At larger values of Q^2, however, the e^-p data lie generally above the e^+p results. This is compatible with a positive (negative) contribution from $x\mathcal{F}_3$ to the e^-p (e^+p) cross section as given in equation (1) and thus predicted by the Standard Model.

The difference between the e^-p and e^+p NC cross section can be used to extract the generalized structure function $x\mathcal{F}_3$ and — since at HERA the dominant contribution to $x\mathcal{F}_3$ comes from the γZ–interference — to evaluate the structure function $xF_3^{\gamma Z}$, which is more closely related to the quark structure of the proton. Figure 3a shows the $x\mathcal{F}_3$ x-dependence as measured by the H1 and ZEUS experiments in six different bins of Q^2. As for the presented analyses the e^-p data have been recorded at a different center-of-mass energy $\sqrt{s} = 318$ GeV than the e^+p data

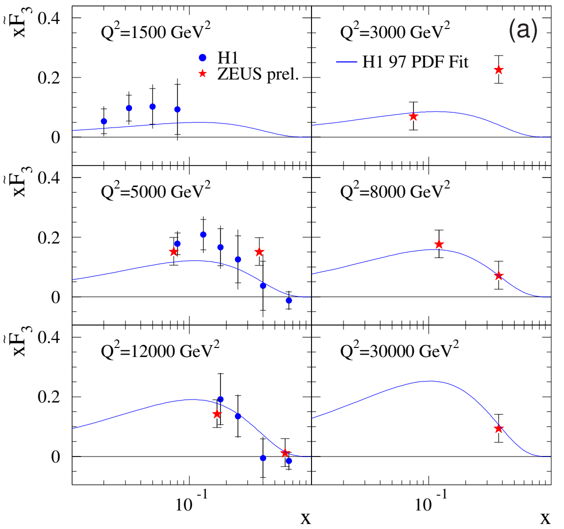

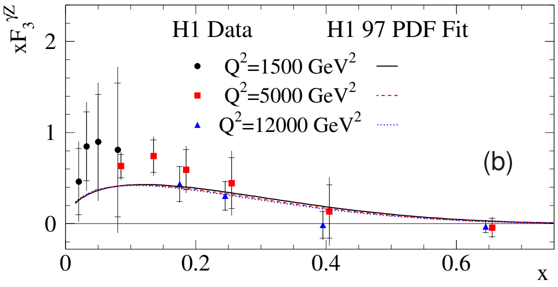

Figure 3: (a) The generalized structure function $x\mathcal{F}_3$, as extracted by H1 and ZEUS. The data are plotted at fixed Q^2 as a function of x. (b) Structure function $xF_3^{\gamma Z}$ as a function of x for three different values of Q^2. All data are compared to predictions from the H1 97 PDF fit [1]. Inner error bars represent the statistical, outer error bars the total error.

taken at $\sqrt{s} = 300$ GeV, $x\mathcal{F}_3$ is evaluated using the following expression

$$\tilde{\sigma}^-_{\rm NC} - \tilde{\sigma}^+_{\rm NC} = x\mathcal{F}_3 \left[\frac{Y_{-\,318}}{Y_{+\,318}} + \frac{Y_{-\,300}}{Y_{+\,300}} \right] - \mathcal{F}_L \left[\frac{y^2_{318}}{Y_{+\,318}} - \frac{y^2_{300}}{Y_{+\,300}} \right] \quad , \tag{6}$$

where the contribution of $\mathcal{F}_L$ can again be neglected. Here, y_{318} and y_{300} are the inelasticities, and $Y_{\pm\,318}$ and $Y_{\pm\,300}$ are the helicity functions as defined above, both evaluated for fixed x and Q^2 and the corresponding center-of-mass energies $\sqrt{s} = 318$ GeV and 300 GeV. The results are in good agreement with the QCD prediction and rise with Q^2 as expected for fixed x due to the propagator dependence (see equation 4).

From these data H1 extracts [2] the structure function $xF_3^{\gamma Z} = 2e_q a_q [q - \bar{q}]$ dividing $x\mathcal{F}_3$ by the factor $-a_e \kappa_w Q^2/(Q^2 + M_Z^2)$; the remaining contribution of order $\mathcal{O}(\chi_Z)$ arising from pure Z-exchange is estimated to be less than 3% and hence neglected. Figure 3b shows $xF_3^{\gamma Z}$ as a function of x for three values of Q^2. The change of $xF_3^{\gamma Z}$ at fixed x over the measured Q^2 range is expected to be very small, as it arises only from QCD scaling violations for a non-singlet structure function. In view of the large experimental errors it is thus possible to directly compare the results at the different Q^2 values.

The presented measurement yields first information on the valence quark content of the proton at high Q^2. As predicted by QCD it is consistent with zero at large x rising to a maximum at $x \approx 0.1$. To quantify the level of agreement between data and theory the following sum rule has been formulated [11] in analogy to the Gross Llewellyn-Smith sum rule [12]: $\int_0^1 F_3^{\gamma Z} dx \approx 5/3$. Averaging the H1 data for different Q^2 at fixed x by taking weighted means, integration yields $\int_{.02}^{.65} = 1.88 \pm 0.44$. The corresponding integral obtained for the H1 97 PDF fit gives 1.11 and is thus found to agree within two standard deviations.

3 Charged Current Reactions

In contrast to neutral current interactions, for which all quark and anti-quark flavours contribute, charged current e^-p (e^+p) reactions probe, in leading order, only down-type (up-type) quarks and up-type (down-type) anti-quarks, as they are mediated by the exchange of the W^- (W^+) boson. Charged current reactions thus allow for flavour-specific investigations of the parton momentum distributions and can provide additional information on the quark content of the proton at high x and high Q^2. Since only the weak interaction contributes, the expression for the

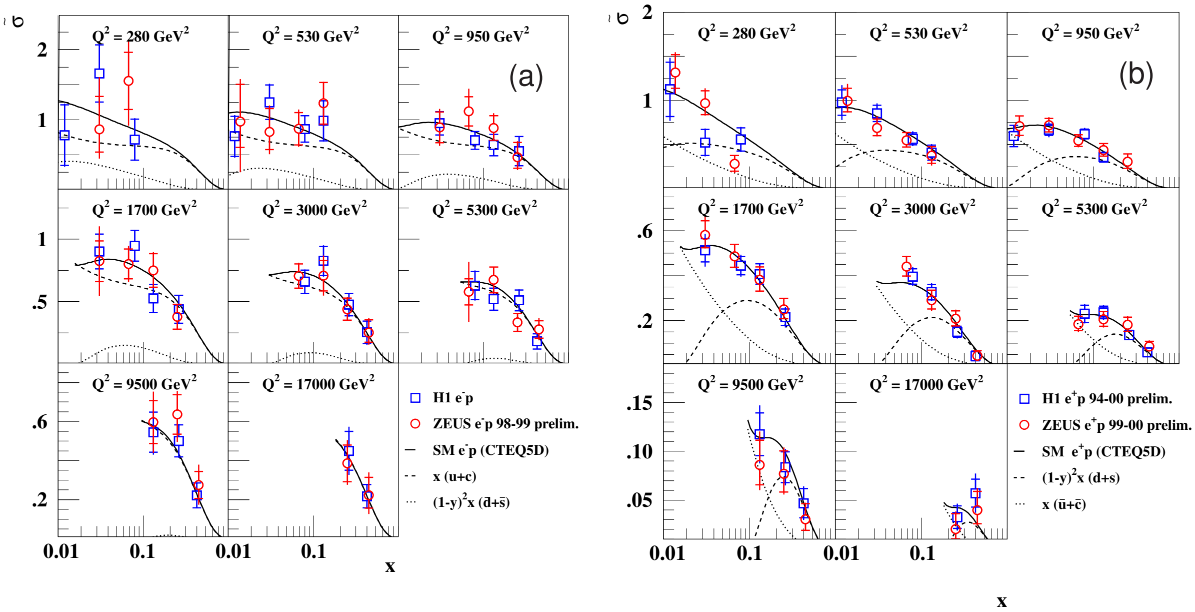

Figure 4: Charged current reduced cross section $\tilde{\sigma}_{\rm CC}(x, Q^2)$ for e^-p (a) and e^+p (b) scattering as measured by the H1 and ZEUS collaborations. The inner error bars represent the statistical error, and the outer error bars the total error of the measurement. The data are compared to the $\mathcal{SM}$ expectation evaluated using the CTEQ5D [8] parton densities. The full lines represent the total cross section predictions; individual contributions from different quark flavours are also shown (dashed and dotted lines) to indicate the sensitivity of the measurement to the valence quark content of the proton at high x.

single-differential charged current cross section at the Born-level [10] can be written in a somewhat simpler form than in the neutral current case:

$$\frac{d^2\sigma^{\pm}_{\rm CC}}{dx\,dQ^2} = \frac{G_F^2 M_W^4}{2\pi x}\frac{1}{(Q^2+M_W^2)^2}\tilde{\sigma}^{\pm}_{\rm CC} \quad , \tag{7}$$

with the reduced cross section given by

$$\tilde{\sigma}^{-}_{\rm CC} = x\left[(u(x,Q^2)+c(x,Q^2)) + (1-y)^2(\bar{d}(x,Q^2)+\bar{s}(x,Q^2))\right] \tag{8}$$

$$\tilde{\sigma}^{+}_{\rm CC} = x\left[(\bar{u}(x,Q^2)+\bar{c}(x,Q^2)) + (1-y)^2(d(x,Q^2)+s(x,Q^2))\right] \quad . \tag{9}$$

Here u, c, d and s are the quark and $\bar{u}$, $\bar{c}$, $\bar{d}$ and $\bar{s}$ the anti-quark distributions. From these equations the sensitivity of CC reactions to the different quark densities becomes evident; at high x, where the contribution from the sea can be neglected, e^-p scattering provides direct access to the u-quark distributions, while positron-proton collisions probe the d-quark content of the proton. This can be seen from figure 4 showing the reduced e^-p and e^+p CC cross section, as measured by H1 [2,4] and ZEUS [3,6], together with the different contributions from quarks and anti-quarks according to the CTEQ5D [8] parton densities.

4 Parton Densities

The full sensitivity of the available ep scattering data is exploited by H1 when using all e^+p and e^-p NC and CC cross sections in a combined NLO QCD fit [4]. From the fit is is possible to extract the dominant valence quark distributions xu_v and xd_v at high Q^2 and high x. The resulting parton densities are shown in figure 5 in the form of a band indicating the estimated uncertainty. The result is compared to the MRST [13] and CTEQ5 [14] parameterizations as well as the H1 97 PDF fit [1], all of which include fixed target data. The uncertainty of the parton densities was

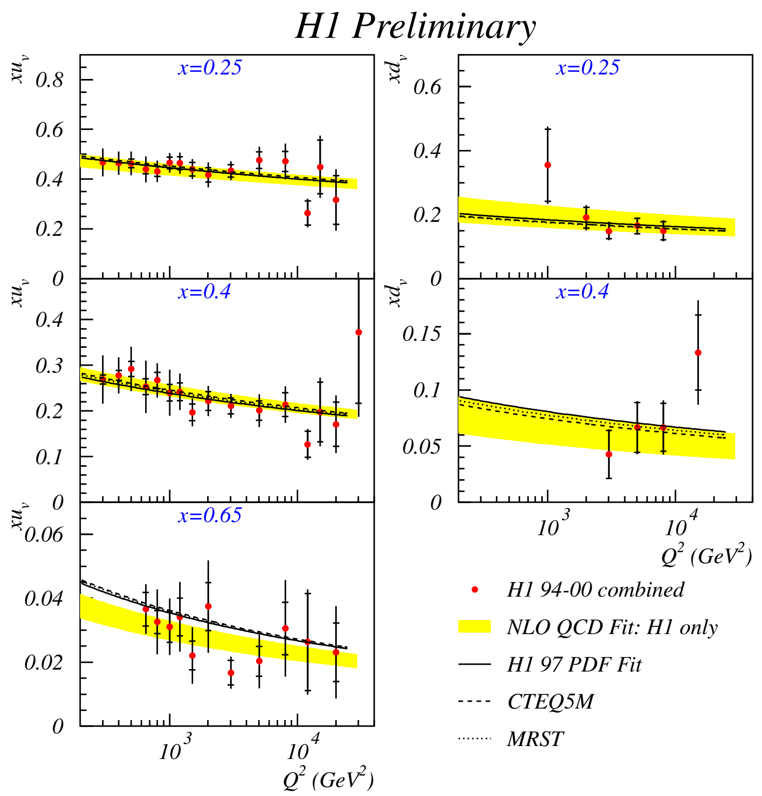

Figure 5: Valence quark distributions xu_v and xd_v as determined with a NLO QCD fit (shaded error bands) using only cross section measurements from H1. Data points have been extracted via a local subtraction method; inner (full) error bars show the statistical (total) error. Other parameterizations extracted using also low Q^2 fixed target data are shown for comparison.

estimated from the experimental errors on the data following the prescription given in [15]. The relative precision of the u-valence varies between 6% for $x = 0.25$ and 10% for $x = 0.65$. The d-valence is essentially constrained by the e^+p CC data only and has a precision of about 20%. The new fit results agree with the other parameterizations within errors. The biggest differences appear at the highest $x = 0.65$ where the H1 fit is about 17% lower with little dependence in the range of Q^2 shown. The difference remains within about two standard deviations. Using a local extraction method [1] data points are derived for the valence quark densities via the relation $xq_v(x,Q^2) = \sigma_{\rm meas}(x,Q^2)\,[xq_v(x,Q^2)/\sigma(x,Q^2)]_{\rm th}$. Here, $\sigma_{\rm meas}$ is the measured NC or CC double differential cross section, while $[\ldots]_{\rm th}$ expresses the theoretical expectation for the ratio of the valence quark density and the cross section. In figure 5 only points with an xq_v contribution of greater than 70% to the total cross section are selected. The extracted parton densities are thus rather independent of the theoretical input as the uncertainty on the dominant valence quark contribution and that of the corresponding total cross section largely cancel in the ratio. Compared to earlier H1 results [1] the data provide an improved statistical precision for the valence quark densities by up to a factor 2; they are in good agreement with the global fits.

5 Future Perspectives

In the year 2000 the HERA machine was significantly upgraded, aiming for a five-fold increase in luminosity [16]. To this end, the final focus magnets for the 920 GeV proton beam are moved closer to the interaction regions of the two ep collider experiments H1 and ZEUS. In addition spin rotators have been installed in order to provide polarized leptons [c].

To adapt to this new situation and to optimally exploit the increased luminosity, H1 and ZEUS both improved and upgraded several detector components. The modifications, in partic-

[c] The HERMES experiment uses such spin rotators already since 1998.

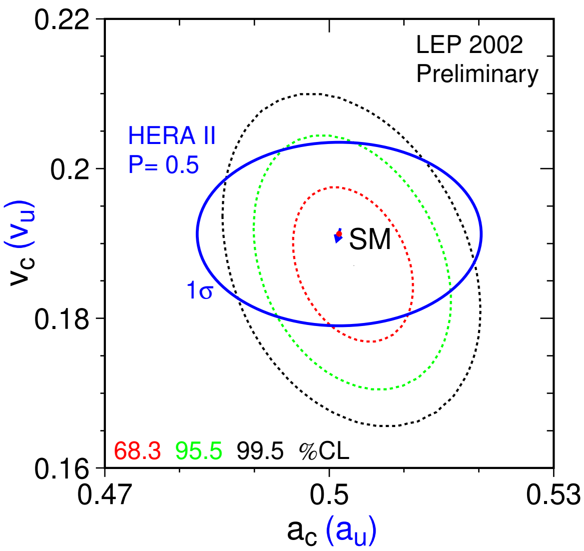

Figure 6: Comparison of the most recent LEP measurement [21] of the Z^0 vector and axial couplings to the c-quark (dashed lines showing the 1σ-, 2σ- and 3σ-contour) with a potential HERA result (full ellipse) for the corresponding u-quark couplings based on 1000 pb^{-1}.

ular, concern the luminosity and polarization measurement, trigger capabilities, upgrade of the silicon vertex detectors and particle identification and reconstruction in the forward direction, i.e. the direction of the proton beam. The physics return from HERA delivering ep collisions with an annual integrated luminosity of $\sim$ 200–250 pb^{-1} and with significant longitudinal polarization is well documented in the proceedings of the HERA Future Physics Workshop [17]. It comprises additional sensitivity to phenomena beyond the $\mathcal{SM}$ such as contact interactions, leptoquarks and flavour changing neutral currents, access to electroweak physics, and the capability to study rare processes in the regime of small momentum transfers Q^2 like deeply virtual compton scattering, onium production or electroproduction of open charm. Here, emphasis shall be put on the investigation of electroweak effects, in particular their utilization to disentangle the neutral current couplings of the u- and d-quark.

A major impact is expected from the provision of polarized leptons. Within the Standard Model NC and CC cross sections are affected not only by the charge of the incoming lepton beam but also by its longitudinal polarization; the reduced cross section for scattering polarized leptons off unpolarized protons is — neglecting the influence of $\mathcal{F}_L$ — given by

$$\tilde{\sigma}^{\pm}_{\{\mathrm{NC,CC}\}} = \tilde{\sigma}^{\pm}_{0,\{\mathrm{NC,CC}\}} \pm \mathcal{P}\,\tilde{\sigma}^{\pm}_{\mathcal{P},\{\mathrm{NC,CC}\}} \tag{10}$$

$$\tilde{\sigma}^{\pm}_{\mathcal{P},\mathrm{NC}} = Y_+\mathcal{F}_2^{\mathcal{P}} \mp Y_-\mathcal{F}_3^{\mathcal{P}} \tag{11}$$

$$\tilde{\sigma}^{\pm}_{\mathcal{P},\mathrm{CC}} = \tilde{\sigma}^{\pm}_{0,\mathrm{CC}} \ , \tag{12}$$

where $\mathcal{P}$ denotes the lepton beam polarization, $\tilde{\sigma}_0$ represents the expression for the unpolarized case ($\mathcal{P} = 0$) as discussed in sections 2 and 3, and $\tilde{\sigma}_{\mathcal{P}}$ contains the effects on the cross section due to a finite value of $\mathcal{P}$. The definitions of $\mathcal{F}_2^{\mathcal{P}}$ and $\mathcal{F}_3^{\mathcal{P}}$ are similar to those in equation 2 with differing coefficient functions [18]. As different choices of the lepton charge and polarization involve different contributions from the different terms in equation 10, data sets taken for various charge/polarization scenarios deliver complementary information on couplings and parton distributions. Neutral current $e^{\pm}p$ data taken with different beam polarizations can thus be used to measure electroweak couplings or to disentangle the individual valence quark densities, which would help to gain important information on the d/u ratio at high x where uncertainties are still large [19,20]. Moreover, by choosing suitable beam configurations $\mathcal{SM}$ processes may be substantially suppressed such that the sensitivity to exotic phenomena is enhanced significantly.

With 250 pb^{-1} of NC data for each lepton charge and a polarization of $\mathcal{P} = \pm 70\%$ it has been estimated that the Z^0 vector coupling v_u (v_d) and the axial vector coupling a_u (a_d) of the u-quark (d-quark) can be measured with accuracies of 13% (17%) and 6% (17%), respectively [18].

Figure 6 shows the expected accuracy of v_u vs. a_u for a more realistic value of $\mathcal{P} = \pm 50\%$ in comparison to the most recent LEP results on c-quark couplings [21]. Both measurements are complementary as they probe different quark flavours. The HERA measurement would thus provide a stringent test of the consistency of the Standard Model.

6 Conclusion

Recent HERA measurements of e^-p and e^+p scattering cross sections at high momentum transfers Q^2 have been presented. The data are in good agreement with the Standard Model predictions and show a clear separation between the e^-p and e^+p cross sections in agreement with the expectation from electroweak theory of a positive (negative) contribution from γZ interference to e^-p (e^+p) scattering. Utilization of the observed differences reveals information on the valence quark densities through extraction of the structure functions $x\mathcal{F}_3$ and $xF_3^{\gamma Z}$ and a combined fit to NC and CC ep scattering data. Future data, to be taken with the upgraded HERA machine during the coming years, will give additional insight into the valence quark content of the proton and allow a precise measurement of the electroweak Z vector and axial couplings of the light quarks.

Acknowledgments

This work was supported by the BMBF (contract no. 05-H1-1PEA/6) and the European Union.

References

1. C. Adloff *et al.* [H1 Collaboration], Eur. Phys. J. C **13**, (2000) 609.
2. C. Adloff *et al.* [H1 Collaboration], Eur. Phys. J. C **19**, (2001) 269.
3. ZEUS Collaboration, "Measurement of high-Q^2 Charged Current Cross Section in e^-p Deep Inelastic Scattering at HERA", EPS 01, Budapest, 2001.
4. H1 Collaboration, "Inclusive Measurement of Deep Inelastic Scattering at high Q^2 in ep Collisions at HERA", EPS 01, Budapest, 2001.
5. ZEUS Collaboration, "Measurement of high-Q^2 Neutral Current Cross Sections in e^+p Deep Inelastic Scattering at HERA", EPS 01, Budapest, 2001.
6. ZEUS Collaboration, "Measurement of high-Q^2 Charged Current Cross Sections in e^+p Deep Inelastic Scattering at HERA", EPS 01, Budapest, 2001.
7. ZEUS Collaboration, "Measurement of high-Q^2 Neutral Current Cross Sections in e^-p DIS and Extraction of the Str. Function xF_3 at HERA", EPS 01, Budapest, 2001.
8. H. L. Lai *et al.* [CTEQ Collaboration], Eur. Phys. J. C **12** (2000) 375.
9. E. Derman, Phys. Rev. D **7**, (1973) 2755.
10. G. Ingelman and R. Rückl, Phys. Lett. B **201**, (1988) 369.
11. E. Rizvi and T. Sloan, arXiv:hep-ex/0101007.
12. D. J. Gross and C. H. Llewellyn Smith, Nucl. Phys. B **14**, (1969) 337.
13. A. D. Martin *et al.*, Eur. Phys. J. C **4** (1998) 463.
14. see e.g. H. L. Lai *et al.*, Phys. Rev. D **55**, (1997) 1280.
15. C. Pascaud and F. Zomer, LAL preprint, LAL/95-05, 1995.
16. W. Bartel *et al.*, Workshop on Future Physics at HERA, Hamburg, 1996.
17. G. Ingelman, A. De Roeck and R. Klanner, "Future physics at HERA", DESY-96-235.
18. R. J. Cashmore *et al.*, Workshop on Future Physics at HERA, Hamburg, 1996.
19. M. Botje, J. Phys. G **28** (2002) 779.
20. S. Kuhlmann *et al.*, Phys. Lett. B **476** (2000) 291.
21. G. Myatt, these proceedings.